Earth and Planetary Science Letters 335–336 (2012) 9–17

Contents lists available at SciVerse ScienceDirect

Earth and Planetary Science Letters

journal homepage: www.elsevier.com/locate/epsl

Puncturing Mars: How impact craters interact with the Martian cryosphere

S.P. Schwenzer [a,j,*], O. Abramov [b], C.C. Allen [c], S.M. Clifford [a,1], C.S. Cockell [d], J. Filiberto [e,2], D.A. Kring [a,3], J. Lasue [a,f,g,4], P.J. McGovern [a,5], H.E. Newsom [h], A.H. Treiman [a,6], D.T. Vaniman [i,7], R.C. Wiens [f]

[a] Lunar and Planetary Institute, USRA, 3600 Bay Area Boulevard, Houston, TX 77058, USA
[b] U.S. Geological Survey, Astrogeology Science Center, 2255 N. Gemini Dr., Flagstaff, AZ 86001, USA
[c] ARES, NASA JSC, Mail code: KA, 2101 NASA Road One, Houston, TX 77058, USA
[d] School of Physics and Astronomy, University of Edinburgh, James Clark Maxwell Building, Mayfield Road, Edinburgh, EH9 3JZ, UK
[e] Southern Illinois University, Geology Department—MC 4234, 1259 Lincoln Dr, Carbondale, IL 62901, USA
[f] Los Alamos National Laboratory, Space Remote Sensing, ISR-2, Mail Stop D-466, Los Alamos, NM 87545, USA
[g] Université de Toulouse, UPS-OMP, IRAP, Toulouse, France
[h] Institute of Meteoritics and Department of Earth and Planetary Sciences MSC03-2050, University of New Mexico, Albuquerque, NM 87131, USA
[i] Planetary Science Institute, 1700 East Fort Lowell Road, Suite 106, Tucson, AZ 85719, USA
[j] The Open University, Earth and Environmental Sciences, Walton Hall, Milton Keynes, MK7 &AA, United Kingdom

ARTICLE INFO

Article history:
Accepted 21 April 2012
Editor: T. Spohn
Available online 14 June 2012

Keywords:
astrobiology
cratering
impact processes
Mars surface
search for extraterrestrial life

ABSTRACT

Geologic evidence suggests that the Martian surface and atmospheric conditions underwent major changes in the late Noachian, with a decline in observable water-related surface features, suggestive of a transition to a dryer and colder climate. Based on that assumption, we have modeled the consequences of impacts into a ~2–6 km-thick cryosphere. We calculate that medium-sized (few 10 s of km diameter) impact craters can physically and/or thermally penetrate through this cryosphere, creating liquid water through the melting of subsurface ice in an otherwise dry and frozen environment. The interaction of liquid water with the target rock produces alteration phases that thermochemical modeling predicts will include hydrous silicates (e.g., nontronite, chlorite, serpentine). Thus, even small impact craters are environments that combine liquid water and the presence of alteration minerals that make them potential sites for life to proliferate. Expanding on the well-known effects of large impact craters on target sites, we conclude that craters as small as ~5–20 km (depending on latitude) excavate large volumes of material from the subsurface while delivering sufficient heat to create liquid water (through the melting of ground ice) and drive hydrothermal activity. This connection between the surface and subsurface made by the formation of these small, and thus more frequent, impact craters may also represent the most favorable sites to test the hypothesis of life on early Mars.

1. Introduction

Our current understanding of what makes an environment habitable includes the availability of a ubiquitous liquid phase which, within the temperature range of life as-we-know-it, is restricted to water (Bennett and Shostak, 2007). Therefore, questions about the former availability of water in the surface and subsurface are key considerations in understanding the potential habitability of Mars and the possibility of finding evidence of fossil or extant life (Tosca et al., 2008; Squyres, 2011). Despite the potential opportunities for the development of life on Mars during the Noachian, physical or chemical evidence of life may be difficult to find. Even the discovery of potential habitable environments does not mean that they were ever actually inhabited (Cockell et al., 2012). Thus, there has been considerable debate concerning the best places to conduct rover-based investigations of possible past or present habitats since these require

* Corresponding author at: The Open University, Earth and Environmental Sciences, Walton Hall, Milton Keynes, MK7 &AA, United Kingdom.
Tel.: +44 1908 659987; fax: +44 1908 655151.
E-mail addresses: s.p.schwenzer@open.ac.uk, schwenzer@lpi.usra.edu (S.P. Schwenzer), oabramov@usgs.gov (O. Abramov), carlton.c.allen@nasa.gov (C.C. Allen), clifford@lpi.usra.edu (S.M. Clifford), c.s.cockell@ed.ac.uk (C.S. Cockell), Filiberto@siu.edu (J. Filiberto), kring@lpi.usra.edu (D.A. Kring), lasue@lpi.usra.edu, jeremie.lasue@irap.omp.eu (J. Lasue), mcgovern@lpi.usra.edu (P.J. McGovern), newsom@unm.edu (H.E. Newsom), treiman@lpi.usra.edu (A.H. Treiman), dvaniman@psi.edu (D.T. Vaniman), rwiens@lanl.gov (R.C. Wiens).
[1] Tel.: +1 281 486 2146.
[2] Tel.: +618 453 4849.
[3] Tel.: +1 281 486 2119.
[4] Tel.: +1 281 486 2195.
[5] Tel.: +1 281 486 2187.
[6] Tel.: +1 281 486 2117.
[7] Tel.: +1 520 622 6300.

0012-821X/$ - see front matter © 2012 Elsevier B.V. All rights reserved.
http://dx.doi.org/10.1016/j.epsl.2012.04.031

both: (1) evidence of a long term-history of aqueous processes, and (2) a way to access the potential habitat by the rover. These considerations suggest that the best opportunity for a rover mission to investigate the subsurface will be in areas where impacts have excavated deep below the surface. In recognition of this, all planned and studied rover missions to the Noachian terrains include the sampling of crater interiors or ejecta. In this study, we investigate how impact craters can penetrate the cryosphere, enabling communication between the surface and subsurface, based on assumptions about the nature of the early Martian climate, calculations of the likely thickness of the cryosphere, models of the minimum sized crater necessary to puncture the cryosphere, and an assessment of the likely mineralogy and fluid composition resulting from such an event. We then consider the implications of these results for enhancing communication between environments above and beneath a cryosphere during the Late Noachian.

1.1. Thermal and hydraulic evolution of the Noachian hydrosphere

Although liquid water is unstable on the Martian surface today, there is abundant geologic evidence that suggests it flowed on the surface in the past. Specifically, the dissection of the planet's Noachian terrains by integrated networks of small valleys is often cited as evidence that early Mars possessed a warmer, wetter greenhouse climate—where rainfall, infiltration and surface runoff were widespread (Masursky et al., 1977; Pollack et al., 1987; Craddock and Maxwell, 1993; Carr, 1999, 2006). VNIR (visible and near infrared) reflectance studies have revealed signatures of chlorides, hydrous silicates and salt hydrates (e.g., Bibring et al., 2005; Carter et al., 2010; Ehlmann et al., 2008a, b, 2009, 2010; Marzo et al., 2010; Milliken and Bish, 2010; Milliken et al., 2010; Murchie et al., 2009a,b; Mustard et al., 2008; Osterloo et al., 2008; Poulet et al., 2005, 2007). Hydrous silicates, such as clays, have been detected from orbit by OMEGA (Observatoire pour la Minéralogie, l'Eau, les Glaces et l'Activité on Mars Express; Bibring et al., 2006) and CRISM (Compact Reconnaissance Imaging Spectrometer for Mars on the Mars Reconnaissance Orbiter; Mustard et al., 2008), while hydrous sulfates have been detected by NASA's two Mars Exploration Rovers (MER) (Arvidson et al., 2007). The combination of this morphological, geochemical and mineralogical evidence makes it clear that liquid water was far more abundant on Mars' surface during the Noachian than at any time since. If so, it suggests that the hydrology of early Mars may have been similar to that of arid environments on present-day Earth, where precipitation, surface runoff and infiltration led to the existence of standing bodies of water and an underlying groundwater system fed by atmospheric recharge.

1.2. Noachian cryosphere

While early Mars may have been warm and wet, the less degraded nature of post-Noachian terrains suggests a geologically rapid transition to less erosive conditions, similar to those that exist on Mars today (Carr, 1999). With the transition to a colder climate, a freezing front developed in the planet's crust, creating a growing cold-trap for both atmospheric and subsurface H_2O—a region known as the cryosphere. The downward propagation of this freezing front, in response to the planet's long-term decline in geothermal heat flux, had two important consequences for the nature of the planet's hydrologic cycle and the state and distribution of subsurface water.

First, as ice condensed within the near-surface regolith it would have significantly reduced communication between any groundwater and the atmosphere and resulted in a distribution of ground ice governed by the thermal structure of the crust, which would have mirrored the first order variations in topography (Clifford, 1993). Assuming reasonable values of crustal permeability (i.e., column averaged values of $\sim 10^{-15}$ m^2 within the top 10 km, Clifford, 1993, Manning and Ingbritsen, 1999), the elimination of atmospheric recharge would have led to the decay of any precipitation-driven influence on the shape of the global water table in $\sim 10^6$–10^8 years. In the absence of major seismic or thermal disturbances of the crust (such as those caused by large impacts, earthquakes and volcanic activity), this would have resulted in an aquifer in effective hydrostatic equilibrium, saturating the lowermost porous regions of the crust. The vertical distance between the base of the cryosphere and the groundwater table may have varied considerably, creating an intervening unsaturated zone whose thickness was maximized in regions of high elevation and minimized (or absent) at low elevation.

Second, as the cryosphere deepened with time, the condensation of ice behind the advancing freezing-front would have created a growing sink for the planet's inventory of groundwater. Where the cryosphere and water table were in direct contact, the groundwater would have frozen to the base of the cryosphere as the freezing front propagated downward with time. However, in many locations throughout the highlands, the vertical distances separating the base of the cryosphere from the water table may have been several kilometers or more. Under such conditions, the depletion of groundwater is expected to have occurred via the thermally induced diffusion of vapor from warmer depths to the colder pores behind the advancing freezing-front (Clifford, 1991, 1993).

2. Cryosphere evolution, impact crater formation and mineral alteration

2.1. Potential extent of the Late Noachian cryosphere

We have used a one-dimensional finite difference thermal model of the subsurface to calculate Martian mean annual surface temperatures and their impact on the depth of the Late Noachian cryosphere. The calculations assume that: (1) the thermal conductivity of ice-saturated basalt varies with temperature following a simple inverse law (Hobbs, 1974; Clifford et al., 2010); (2) the mean value of Late Noachian geothermal heat flux can be deduced from estimates of the rheologic properties of the Martian lithosphere necessary to support the relief of the Noachian topography (McGovern et al., 2004); and (3) the variations in Martian obliquity and orbital eccentricity were comparable to those of today (an assumption whose validity is largely dependent on the developmental state of Tharsis at that time; Ward, 1979).

Fig. 1 illustrates the variation in the depth of the cryosphere as a function of latitude based on the average and extreme obliquity and orbital eccentricity values of Laskar et al. (2004), combined with an assumed Noachian geothermal heat flux of 60 mW m^{-2} (McGovern et al., 2004), and three groundwater freezing temperatures—corresponding to pure water (273 K), a eutectic solution of sodium chloride (252 K) and a eutectic solution of magnesium perchlorate (203 K).

In the absence of dilution associated with the infiltration of rainfall or meltwater, Martian groundwater is expected to be highly saline—a natural consequence of the leaching of soluble minerals from the host rock by groundwater over the hundreds of million years the two have been in intimate contact. Thus, the 252 K and 203 K eutectics were chosen to represent the plausible range of salt-induced freezing point depression on Mars. For example, sodium chloride is the main constituent of seawater on Earth and its eutectic of 252 K could be easily reached as an

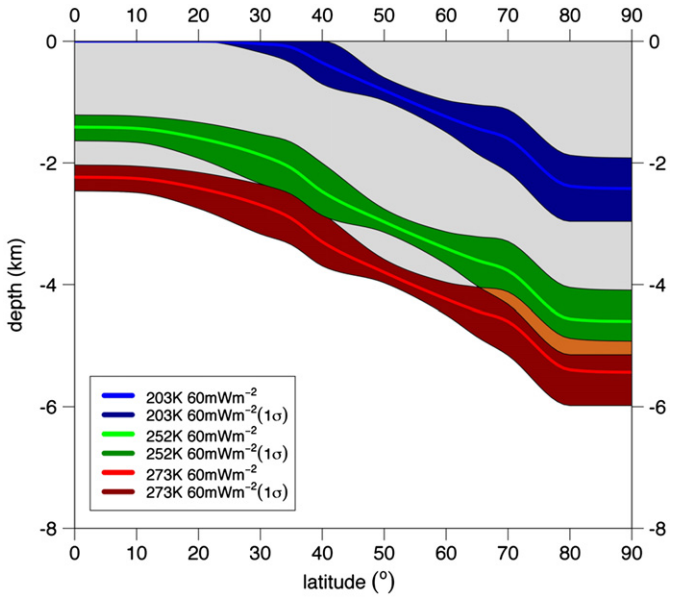

Fig. 1. Depth of the Martian cryosphere as a function of latitude based on the assumption that the crust has a temperature-dependent thermal conductivity equivalent to that of water ice, a geothermal heat flux of 60 mW m^{-2} and obliquity and orbital eccentricity characteristics given by the probability distribution functions of Laskar et al. (2004). Solid lines represent cryosphere depths calculated from the average values of obliquity and orbital eccentricity, while the shaded region around each correspond to the maximum and minimum depths calculated based on the 1σ high and low extremes of obliquity and orbital eccentricity. The three isotherms depicted correspond to the freezing points of pure water (273 K in red), a eutectic solution of sodium chloride (252 K in green) and a eutectic solution of magnesium perchlorate (203 K in blue).

initially more dilute reservoir of salt-rich groundwater was depleted as groundwater was progressively cold-trapped within the thickening cryosphere. Similar values might also be obtained by more dilute solutions of magnesium chloride (238 K eutectic) and calcium chloride (218 K eutectic) or by multi-component mixtures of these and other salts (Clark and Van Hart, 1981). The 203 K eutectic of magnesium perchlorate was chosen as a limiting value because it has the greatest freezing point depression associated with any salt yet found on Mars (Morris et al., 2009; Hecht et al., 2009).

The resulting calculated maximum depth of the cryosphere (based on the assumption of a pure water freezing point) varies from ~2.3 km near the equator up to ~5.6 km near the poles, where mean annual temperatures are significantly colder due to the combination of lower insolation and the higher albedo of the seasonal and perennial polar ice deposits (which are assumed to have an extent comparable to that of today's). For a freezing point appropriate to a saturated solution of magnesium perchlorate (i.e., 203 K), the extent of the cryosphere is much reduced, reaching a maximum thickness at the poles of ~2.5 km and diminishes with lower latitudes until it completely disappears at latitudes of less than ~30–35° (where mean annual temperatures exceed the assumed perchlorate-depressed freezing point of groundwater).

For the cryosphere calculations, we considered the maximum estimate of cryosphere thickness at both the equator and poles and will use our equatorial results for the melt-through calculations (see Section 2.1). Assuming a 20 Myr obliquity history equivalent to the nominal model of Laskar et al. (2004), we calculate a 20 Myr mean equatorial surface temperature of 216 K which yields a local cryosphere thickness of ~2–2.5 km, assuming a geothermal heat flow of 60 mW m^{-2} and a solute-free groundwater freezing point of 273 K. At the poles, we calculate a mean surface temperature of 157 K which (assuming the same values of geothermal heat flow and freeing point) yields a maximum predicted thickness of the polar cryosphere of ~5–6 km.

2.2. Water content in the Noachian cryosphere

To estimate the volume of H_2O that was cold-trapped into the Noachian cryosphere we calculate the pore volume of the crust between the Martian surface and the base of the cryosphere. We assume a surface porosity of 0.20 and a 1/e decay constant of 2.82 km based on the porosity vs. depth relationship of Clifford (1993). We calculate that a Noachian cryosphere could have cold-trapped the equivalent of ~200 m ($\pm$125 m) GEL (global equivalent layer) of H_2O as ground ice. Subtracting this quantity from Carr's (1986, 1996) ~500–1000 m GEL estimate of the total planetary inventory of water suggests that, by the end of the Noachian, ~300–800 m GEL of groundwater still survived beneath the thickening cryosphere.

Geographic variations in geothermal heat flow, as well as the heat produced by volcanic activity and impacts, could have significantly affected both the extent of the cryosphere and the energy available to drive the hydrothermal circulation of water from deep aquifers. Our cryosphere thickness calculations raise the question of whether the confinement of those aquifers would have been affected by the thermal disturbances associated with mid- and larger-sized impacts. We now investigate the minimum size range of craters necessary to puncture the late Noachian cryosphere and the potential effects that associated changes in temperature and water flow would have had on local mineralogy.

2.3. Modeling an impact's aftermath

2.3.1. Interaction of impact-deposited heat with the cryosphere

An impact can deposit a huge amount of energy into the local crust that scales with the mass and square of the velocity of the impactor—much of which is turned into heat. Post-impact temperature distributions can be determined analytically (e.g., Abramov and Kring, 2005; Abramov and Mojzsis, 2009). The initial shock-induced heating is calculated using the Murnaghan equation of state for specific waste heat (ΔE_W) (Kieffer and Simonds, 1980):

$$\Delta E_w = \frac{1}{2}\left[PV_0 - \frac{2K_0V_0}{n}\right]\left[1-\left(\frac{Pn}{K_0}+1\right)^{-1/n}\right] + \frac{K_0V_0}{n(1-n)}\left[1-\left(\frac{Pn}{K_0}+1\right)^{1-(1/n)}\right] \quad (1)$$

where P is the peak shock pressure, K_0 is the adiabatic bulk modulus at zero pressure (19.3×10^9 Pa for basalt), n is the pressure derivative of the bulk modulus (5.5 for basalt), and V_0 is the specific uncompressed volume ($1/\rho_0$); all of these parameters are well established for basalt, the assumed target material. Shock pressure P drops off with distance r from the impact center, which is at a depth approximately equal to the impactor radius (Pierazzo and Melosh, 2000), according to the power law:

$$P = A\left(\frac{r}{R_{pr}}\right)^{-k} \quad (2)$$

where R_{pr} is the radius of the projectile, k is the decay exponent, and A is pressure at $r=R_{pr}$. The decay exponent k varies as a function of impact angle (Pierazzo and Melosh, 2000) and velocity (Ahrens and O'Keefe, 1987), and can be estimated as $k\approx-0.625\log(U)-1.25$,

where U is impact velocity in km/s, for the vertical impacts modeled here (Ahrens and O'Keefe, 1987).

A depends on target and impactor properties, and is estimated by Collins et al. (2002) as

$$A = \frac{\rho v_i^2}{4} \tag{3}$$

where ρ is impactor and target density, both of which are assumed to be 3000 kg m^{-3}, consistent with a rocky asteroid striking a basaltic crust, and v_i is impact velocity.

To obtain the temperature increase, the specific waste heat ΔE_w is divided by the heat capacity of the target rock, which is 800 J kg^{-1} K^{-1} for basalt. To obtain the subsurface temperature distribution, geothermal temperatures are then added to the impact-deposited heat. Fig. 2 shows a final temperature distribution for a ~30-km diameter complex crater, which is in good agreement with hydrocode models of impacts on Mars (Pierazzo et al., 2005).

Once the subsurface temperature distribution is calculated (see Section 2.1), the volume of the transient crater, which represents material vaporized or ejected by the impact, is removed. The transient crater diameter, as measured at the pre-impact surface, is calculated using the Pi-scaling laws (e.g., Holsapple and Schmidt, 1982; Schmidt and Housen, 1987):

$$D_{tc} = 1.16 d^{0.78} v_i^{0.44} g^{-0.22} \tag{4}$$

where d is the impactor diameter, v_i is the impact velocity, and g is the acceleration of gravity, which on Mars is 38% of that on Earth. The above expression is valid only if the impactor and target density are assumed to be the same (here, 3000 kg/m^3). The rim-to-rim diameter of the transient crater is above the pre-impact surface and ~1.2 times larger than D_{tc} (Melosh 1989). The depth of the transient crater is estimated by multiplying the rim-to-rim diameter of the transient crater by 0.25 (Melosh, 1989).

The rim-to-rim diameter of the final crater is calculated using the following relationship (Abramov and Kring, 2005):

$$D = 0.91 \frac{D_{tr}^{1.125}}{D_Q^{0.09}} \tag{5}$$

where D is the rim-to-rim diameter of the final crater, D_{tr} is the rim-to-rim diameter of the transient crater, and D_Q is the simple-to-complex transition diameter, ~8.4 km for Mars (see Abramov and Kring, 2005 for details). Using a smaller D_Q of $5.1^{+3.1}_{-1.9}$ km for Mars (Pike, 1988) does not significantly change the minimum size of the transient crater that punctures the cryosphere. It does change the size of the final crater resulting from relaxation of the transient cavity. We chose to use 8.4 km, which results in a slightly larger crater, but is also consistent with the Pike (1988) value for crystalline target material.

Two cryospheric thicknesses are modeled using the thermal penetration model described above: 2 km, which represents the approximate depth of the equatorial cryosphere, and 6 km, which represents the approximate depth of the polar cryosphere. In addition, a 6-km thick cryosphere may have been possible in the equatorial regions if the heat flow was significantly lower than the 60 mW m^{-2} estimated by McGovern et al. (2004), as has recently been suggested by Hahn et al. (2011). For each of the two cryosphere thicknesses, two modeling scenarios are presented: (i) a case with the subsurface being composed of 100% basalt and no water ice, allowing Eq. (1) to be applied explicitly, yielding the minimum crater sizes and projectile diameters needed to thermally penetrate the cryosphere, and (ii) a case with a cryosphere containing 80% basalt and 20% water ice by volume. Because no equation of state is currently available for a two-component ice-rock mixture, we calculate the energy deposited by the impact using shock parameters for basalt, but take into account the heat capacity and latent heat of melting of the water ice component when calculating the final temperature distribution.

We calculate that a 6 km-thick target (100% basalt, no ice) can be thermally penetrated, or brought above the melting temperature of water ice, by an impactor as small as 0.89 km in diameter. The rim-to-rim diameter of the resulting transient crater is 10.8 km; the rim-to-rim diameter of the final crater is 14.0 km (Fig. 3). For comparison, a 2 km-thick basalt layer at the same low surface temperature can be thermally penetrated by an impactor of only 0.30 km diameter. The transient crater diameter in this case is 4.6 km, resulting in a final crater diameter of 5.3 km. In this example, there is no ice, which further decreases the minimum impactor size needed to "thermally penetrate" this layer.

In addition, we estimate the minimum impactor size needed to thermally penetrate a 6-km thick, ice-rich cryosphere containing 80% basalt and 20% water ice by volume. The energy consumed by the latent heat of melting of the ice, as well as increased heat capacity, requires a larger impactor to thermally penetrate the

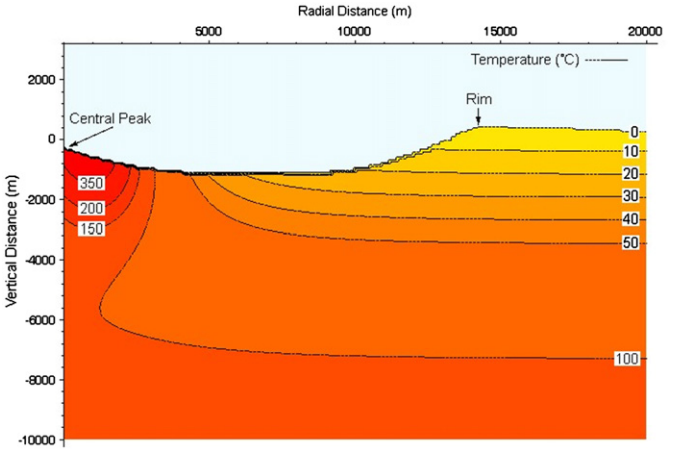

Fig. 2. Post-impact temperature distribution in a 29-km crater on Mars immediately after an asteroid impact, calculated using the Murnaghan equation of state. Black lines are isotherms, labeled in degrees Celsius. Yellow colors indicate temperatures below 30 °C, orange colors between 30 and 100 °C and red colors correspond to temperatures above 100 °C. In addition to shock-deposited heat, heat from the central uplift and the geothermal gradient is included. From Abramov (2006).

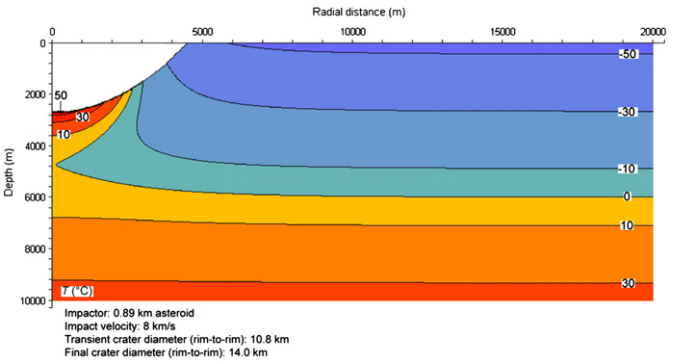

Fig. 3. Post-impact temperature distribution around the transient cavity of a relatively small (10.8 km transient diameter; 14.0 km final diameter) km crater on Mars immediately after the impact. The impactor modeled was a 0.89 km diameter asteroid. Black lines are isotherms, labeled in degrees Celsius. Blue colors indicate temperatures below freezing, yellow colors correspond to temperatures between 0 and 50 °C, and higher temperatures are indicated by red colors. Note the connection between the liquid water caused by the impact with the deep, fluid aquifer indicated by the gap between the zero degree isotherm and the center of the crater.

target. The minimum projectile diameter required is 1.8 km, resulting in a transient crater with a diameter of 19.1 km and producing a final crater with a rim-to-rim diameter of 26.6 km. For a 2-km thick, 80% basalt, 20% water ice cryosphere, the minimum projectile diameter required is 0.60 km, resulting in a transient crater with a diameter of 8.0 km and producing a final crater with a rim-to-rim diameter of 9.9 km. It should be noted that for a crater this small, the resulting subsurface heating is insufficient to melt the ice, and the thermal penetration depth is equivalent to the depth of the transient crater.

Within an area of $\sim 9 \times 10^6$ km^2 of the Martian highlands, Strom et al. (2005) counted ~850 craters with diameters of ~10 km, as well as numerous larger impacts. Overall, there are ~3850 impacts with diameters equal to or larger than 10 km (Barlow, 1990), the majority of which are believed to have formed between 4.2 and 3.9 Ga (Kring and Cohen, 2002; Norman and Nemchin, 2012). The effects of much larger impacts into ice bearing target have been modeled before and result in hydrothermal systems, which might be restricted to the central area of the crater (Barnhart et al., 2010; Ivanov and Pierazzo, 2011). Our results, however, indicate that, even for the maximum polar cryosphere thickness of 6-km, relatively small impactors can result in the frequent melt-through for a predominantly basaltic crust. A thinner cryosphere, such as the one that may have existed earlier in Martian geologic history (i.e., in the absence of a massive early greenhouse), would be penetrated even 'more easily'. The effects of such impacts on the cryosphere include the melting of ice and fracturing of rock—resulting in the production of liquid water and the exposure of more fresh surface area that would be susceptible to formation of alteration minerals.

2.3.2. Alteration mineralogy of low temperature hydrous alteration

Based on the temperatures and pressure of impact-crater-driven water circulation, we use CHILLER to calculate the alteration caused by low temperature fluids in contact with Martian rock compositions. CHILLER (Reed and Spycher, 2006) calculates solids, solutions, and gaseous phases in equilibrium with each other at given pressure and temperature. The input data for our calculations are a dilute fluid (mole kg^{-1} of species; Table 1), temperature (1–20 °C here) and unaltered Martian rock composition. Since even modest sized craters can reach deep into the Martian subsurface (Figs. 2 and 3) we assumed a plutonic rock, i.e., a lherzolithic shergottite as our target composition—Martian meteorite LEW88516 (Table 1). The fluid for our calculations is a dilute brine that we have previously used the calculate Martian alteration assemblages (e.g., Schwenzer and Kring, 2009a, b; Filiberto and Schwenzer, 2011; Bridges and Schwenzer, 2011; Schwenzer and Bridges, 2011). This allows us to compare and contrast our results to our previous models: the alteration of LEW88516 at higher T (150 °C) (Schwenzer and Kring, 2009a), and the alteration of the Lafayette martian meteorite (intermediate T between 100 and 70 °C; Bridges and Schwenzer, 2011; Schwenzer and Bridges, 2011). We also modeled pure olivine from LEW88516 (Table 1, Fig. 4). We discuss below the results of the models following the chronology of a post-impact scenario, starting from fresh fractures and proceeding through an evolving alteration system.

The impact leaves the target site fractured and with many fresh, unaltered surfaces. Melting of ice (Fig. 3) will cause water flow into these new sites. Reaction kinetics at low temperature are slow; thus it is assumed that the inflowing water reacts with the freshly exposed surfaces only, which will keep effective water to rock ratio (W/R) at high levels. Under these effectively high W/R conditions (W/R of 10,000 and 1000, Fig. 4) di-octahedral smectite, Mg-nontronite (e.g., $Mg_{0.33}Fe_4(Al_2Si_6O_{20})(OH)_4.nH_2O$), may form on surfaces and in cracks along with goethite and pyrite. Formation of this assemblage is independent of the oxidation state of the host rock, as can be demonstrated by comparing alteration of a rock with all Fe as FeO to alteration of a rock with 10% of Fe as Fe_2O_3 (Fig. 4). With W/R ratios of 10,000–1000, differences between models with varying oxidation state are minor. With time, more host rock is expected to dissolve into

Table 1
Input chemistry for LEW88516, which is a weighted mean of the analyses of Dreibus et al. (1992), Warren and Kallemeyn (1996), and two analyses by Gleason et al. (1997). Olivine composition is from Gleason et al. (1997). Water chemistry is derived by taking the Ca-concentrations of thermal water venting the Deccan trap basalts (Minissale et al., 2000) and adjusting Fe and Mg according to their ratios in LEW 88516. HCO_3^- is derived by equilibrating today's Martian atmosphere with the fluid, SO_4^{2-} is adjusted to the S concentration in LEW 88516, and Cl^- is used for charge balance.

Oxide	LEW 88516 (wt%)	Olivine (wt%)	Ion	Starting brine (mole kg^{-1})
SiO_2	44.79	36.47	Fe^{3+}	9.19E−3
TiO_2	0.40	0.02	Mg^{2+}	20.53E−3
Al_2O_3	3.29	0.02	Ca^{2+}	2.5E−3
Cr_2O_3	0.88		HCO_3^-	1.68E−5
FeO	19.92	31.76	SO_4^{2-}	2.85E−3
MnO	0.49	0.64	Cl^-	6.80E−1
MgO	25.01	31.60		
CaO	4.22	0.01		
Na_2O	0.54	0.01		
K_2O	0.03	0.01		
P_2O_5	0.39			

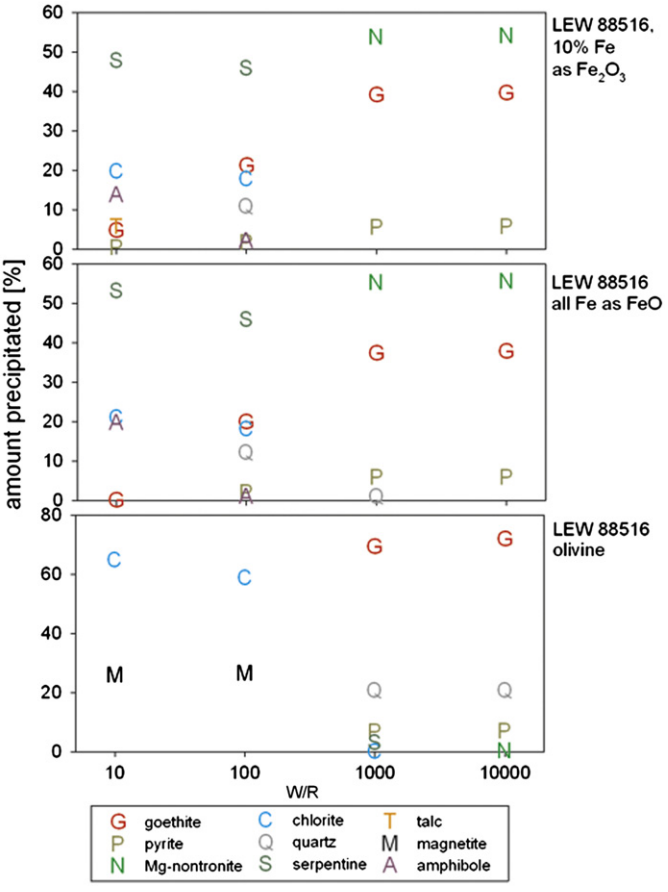

Fig. 4. Alteration mineral abundances related to water to rock ratio (W/R). Shown are four W/R ratios: 10, 100, 1000, and 100,000. CHILLER calculations for 1 °C and 1 bar. Note the difference between the low and high W/R ratios.

the brine, which causes the activity of dissolved species to increase.

At W/R of 100, serpentine is the most abundant phase, but goethite still makes up 20% of the alteration assemblage. Chlorite [clinochlore, e.g., $Mg_{9.98}Al_{2.00}Fe_{0.02})_{12}(Al_2Si_6O_{20})(OH)_{16}$] is the third most abundant phase. The relative abundances of chlorite, smectite and serpentine vary with the variation of temperature and other parameters such as oxidation state. For example, the nontronite–serpentine assemblage found in the nakhlites (Changela and Bridges, 2010) has formed under oxidizing, intermediate-temperature (~70 °C) conditions after an initial stage of higher-*T* (~100 °C) carbonate formation (Bridges and Schwenzer, 2011, Schwenzer and Bridges, 2011). Moreover, the availability of critical species (e.g., Al for smectite formation) varies with varying target composition and controls the precipitated alteration assemblage (comp. Fig. 4).

At W/R of 10, serpentine and chlorite together make up about 70% of the alteration assemblage with amphibole as the third most abundant phase. At this point, noticeable differences between different oxidation states do occur. In the more reducing case, no talc is formed, but amphibole abundances are increased. With the low temperatures reached after small impacts, we do not expect the system to form amphiboles, but serpentinization can occur. Since the serpentinization reaction is exothermic, the formation of serpentine can add heat to the system (Piranjo, 2009), potentially extending the lifetime of warm conditions. Overall, smectites and oxides dominate the alteration products. This is in accordance with laboratory experiments (Harder, 1976; Grauby et al., 1994), terrestrial nontronite formation (e.g., Dekov et al., 2007), and observations in the nakhlite Martian meteorites, which have recently been suggested to be altered by an impact-generated hydrothermal system (Changela and Bridges, 2010). The model fluid for the above models did not contain sufficient amounts of dissolved CO_2 to produce an initial carbonate-forming phase. However, from models on ALH84001 in contact with a fluid with 0.5 mol L^{-1} dissolved CO_2 (Schwenzer and Kring, 2009b) and the Lafayette composition (Bridges and Schwenzer, 2011, Schwenzer and Bridges, 2011) we expect siderite, Mg-siderite, and Mg-Ca-siderite to form in the presence of dissolved CO_2.

To explore the alteration parameter space further, we assume only olivine dissolution, since olivine-rich lithologies (10–20 vol %) have been reported on the surface of Mars (e.g., Koeppen and Hamilton, 2008; Edwards et al., 2008) and meteorite LEW88516 contains 57% olivine while NWA 2737 and Chassigny are >90% olivine (Floran et al., 1978). The alteration products of an olivine-rich substrate would be significantly different from alteration of a basaltic rock. At high W/R oxides, silica and pyrite are formed almost exclusively: ~70% goethite is accompanied by ~20% quartz and lesser but significant percentages of pyrite. At lower W/R chlorite and magnetite with some trace phases such as graphite (from $\sim 0.3 \times 10^{-4}$ mol $L^{-1}H_2CO_3$ in the starting solution) precipitate (Fig. 4). Note that olivine contains no Al; therefore the chlorite is Al-poor: $(Mg_{11.98}Al_{0.006}Fe_{0.014}Mn_{tr})_{12}(Si_8O_{20})(OH)_{16}$. The dissolution of pure olivine produces a gas phase that contains H_2. At a W/R of 100, 0.1 mol H_2 is produced per kg dissolved rock and at W/R of 10 this increases to 1.3 mol per kg of dissolved rock. In the presence of CO_2 and magnetite (Zolotov and Shock, 1999) methane might form (Oze and Sharma, 2005; Schwenzer, 2011).

3. Implications for habitability

Freezing, formation of a cryosphere, and impact-related processes can change the habitability of a site considerably. We now discuss these effects starting with the smallest scale, i.e., mesoscopic mineralogic changes, and expand to crater-, regional- and planet-wide effects that might affect the habitability of sites, e.g., pathways for the transport of metabolizing or dormant species between habitats, mineralogical inventory, the occurrence and availability of biologically important elements, and how such regions would be best explored.

3.1. The smallest scale: mineralogical changes

The impact-generated temperature increase and subsequent water flow cause several important changes in the mineralogy of the site. Above we assumed that the target contained mainly 'magmatic' minerals such as olivine and pyroxene with no ion-exchange, water storage capabilities, or structurally bound water; however, the impact-generated alteration changes the mineralogy to include minerals with both exchange capabilities and structurally bound water. If LEW88516 is altered at W/R of 1000, this will cause the following assemblage to form (Fig. 4): Mg-nontronite (53.84 wt%; $Mg_{0.33}Fe_4(Al_2Si_6O_{20})(OH)_4.nH_2O$), goethite (39.01 wt%), pyrite (5.57 wt%), quartz (0.96 wt%), and Cl-apatite (0.62 wt%; $Ca_5(PO_4)_3Cl$). Nontronite and goethite together introduce ~12 wt% structurally bound 'water' in the form of OH-groups, which can be released in dehydration reactions (Deer et al., 1992) but are stable against freezing, transport or evaporation. Nontronite can take up water (swelling) and cations (ion exchange capability) in its interlayers (Deer et al., 1992; Stucki, 2006). Thus, smectites provide water storage capabilities protecting the site from rapid desiccation and may contain cations available for exchange by subsequent processes. In addition, the alteration process changes redox conditions (Bridges and Schwenzer, 2012) and the chemical speciation of biologically essential elements such as sulfur and phosphorus.

An important issue for the geologic distribution of impact generated hydrothermal mineral assemblages in large craters on Mars is the dependence of their formation on the water/rock ratio. The water/rock ratio is expected to vary to a much larger extent than the final thermal environment due to natural variations in porosity, transmission of water along faults, and other structural features associated with real geological structures. Alteration minerals can also be physically transported by numerous mass-transport processes (e.g., landslides, water and eolian transport) during their formation and throughout the later history of a crater. Therefore, theoretical modeling of the formation of alteration minerals is unlikely to predict the natural distribution of alteration minerals around actual Martian craters.

If life was present, the described mineralogical changes could have worked in its favor by liberating ions, but also by the H_2 formed, pyrite, and – more generally – specific redox series, e.g., Fe^{2+}/Fe^{3+}, that could have been involved in electron donor/acceptor reactions as potential sources of energy for organisms (Varnes et al., 2003). The liquid phase in equilibrium with the alteration assemblage at W/R=1000 is a diluted brine (pH 6.6) that contains ions relevant for biologic activity, for example Ca^{2+} (0.32×10^{-2} mol L^{-1}), Mg^{2+} (0.26×10^{-1} mol L^{-1}), K^+ (0.64×10^{-5} mol L^{-1}), and Na^+ (0.17×10^{-3} mol L^{-1}). Therefore, the post-impact site contains a fluid system that could deliver essential elements for life.

3.2. Local scale: craters as special sites for the search for traces of fossil or recent life

Impacts have been proposed as a natural excavation process in the search for the evidence of life (Newsom et al., 2001; Cockell and Barlow, 2002). On Mars, ~40 impact basins with diameters >1000 km are thought to have been produced prior to ~3.9 Ga (Horner et al., 2009), many of which might have formed between 4.2 and 3.9 Ga (Kring and Cohen, 2002; Norman and Nemchin,

2012). Given a water-rich Mars, such large impacts are expected to have excavated deep into the crust and produced hydrothermal systems with lifetimes up to 10 Ma (Abramov and Kring, 2005). Smaller craters created transient increases in temperature for much shorter timescales and any hydrothermal or mineralogical effects associated with them were far smaller. But smaller craters are much more numerous than larger ones, both in the Noachian and later in the planet's history, and can provide connections between a subsurface habitat and the surface—or, through heating of local target rocks, revive habitable sites by producing liquid water. Looking for evidence of life in small- to mid-sized craters is therefore promising because of their former potential to support life (through the production of meltwater, increased availability of biologically important ions, and prolonged heating of the crust), the possible connections they may have created between the surface and subsurface aquifers/habitats, and for the window they provide into subsurface geology, geochemistry, and the cryosphere.

3.3. Regional scale: cryosphere

The interaction of the Martian cryosphere with impact crater formation processes has been considered for the case of fluidized ejecta blankets (Barlow 2005, 2006; Reiss et al., 2006; Osinski, 2006) and very recent impacts (Byrne et al., 2009). Small, meter-sized craters have formed on Mars throughout its history up to the present. In recent craters, ice has been observed but sublimates rapidly when directly exposed to the Martian atmosphere (Byrne et al., 2009). However, craters surrounded by lobate ejecta blankets occur in association with impacts >1 km in diameter and are present in all terrains, spanning Martian geologic time (Allen, 1979; Barlow, 2005, 2006; Osinski, 2006). In detail, the smallest craters with lobate ejecta blankets are observed to be about 3 km at the equator and <1 km at the poles (Barlow, 2006). As volatiles are apparently linked to their formation, they have been used to track the deepening of the top of the ice-table in the Hesperian (Reiss et al., 2006). We calculate 5.3 km and 14 km crater diameters can thermally penetrate the cryosphere at the equator and poles, respectively. However, penetration of the cryosphere is not required to mobilize volatiles in an ejecta blanket. At the end of the Noachian, with the ice-table close to the surface, even small impacts were capable of melting ice and larger ones could have initiated long-lived hydrothermal systems (Section 2.2). While the growth of the cryosphere over time would have resulted in the further isolation of the potentially habitable subsurface from the dry and hostile environment at the surface, impact craters should have punctured or melted through this barrier quite frequently, providing pathways for two-way (and potentially long-enduring) exchange.

For impacts that occur at lower elevations, where the hydraulic head of the subpermafrost aquifer lies higher than the local surface elevation, the thermal penetration of the cryosphere may result in artesian discharge of a significant volume of groundwater, depending on the local value of crustal permeability, the salinity of the groundwater, and the potential for advective heat transport by groundwater originating from warmer regions within the aquifer. However, at elevations where the local hydraulic head lies below the local surface elevation, the potential for groundwater discharge rests solely on the vigor of local hydrothermal convection—in response to the interaction of impact melt with the surrounding water-rich crust.

Of course, if Martian groundwater at this time consisted of a eutectic solution of magnesium perchlorate, then it would have had a freezing point lower than the mean annual temperature of the entire equatorial region, lying between $\pm 30^{\circ}$ latitude. Under these conditions, the local aquifer would be unconfined—allowing water to discharge and pond on the surface until local hydraulic equilibrium was achieved. Under these conditions, impact-generated thermal disturbances – sufficient to drive the hydrothermal convection of groundwater – could potentially occur in association with much smaller craters than the ~ 5 km diameter necessary to penetrate the maximum estimated thickness of the equatorial Noachian cryosphere.

Later in the planet's history, the thermodynamic instability of near-surface ground ice at equatorial latitudes would have led to the progressive desiccation of this region – from as little as a few meters potentially down to km-depths—a conclusion supported by the geologic evidence (e.g., Craddock and Howard, 2002). Under these conditions, the thermal disturbance associated with a small impact may have been confined to the desiccated near-surface—yielding little or no meltwater to create a transiently habitable environment, unless the disturbance was sufficient to liberate water from previously formed hydrated minerals.

The occurrence of large impacts early in Mars history would have caused areally extensive fracturing of the crust – and to great depths – enhancing the likelihood of hydraulic communication between deep subpermafrost aquifers (Clifford, 1993), which would have enabled the transport of both biota and mineral-derived soluble nutrients from one habitable environment to another. Terrestrial fracture networks, within and beneath artic permafrost, serve an analogous function—harboring sulfate-reducing microorganisms and other anaerobic taxa that can grow within the cold, saline conditions of the permafrost (Onstott et al., 2009).

4. Conclusions

Whether the Noachian climate was warm or cold, the formation of impact craters on a water-rich Mars is expected to have resulted in the development of widespread hydrous and hydrothermal activity. By the end of the Noachian, the Martian climate appears to have undergone a geologically rapid transition to its present cold and arid state. Even under these deep frozen surface conditions, large impacts are capable of producing hydrothermal activity and thus keeping water a liquid for durations up to 10 Ma. Thermal disturbances arising from small impacts may also result in the production of meltwater, although their smaller volume and temperature rise (some tens of degrees) may yield substantially smaller volumes and liquid lifetimes. While changes to the local hydrologic regime can cause alteration in both cases, the resulting mineralogy will differ due to the different temperature and pressure conditions surrounding the impact site. The transient occurrence of liquid water associated with the large number of Noachian craters created a broad range of potentially habitable environments. Even if climatic conditions at the end of the Noachian were as cold as they are today, the resulting ~ 2–6 km-thick cryosphere would have been readily and frequently penetrated by impactors, providing hydraulic links between the impact-generated hydrothermal systems and any underlying regional or global aquifer. Alteration models, starting with barren basaltic compositions, produce hydrous minerals that on Earth are characteristic of and important to terrestrial habitable environments. The cumulative result of many impacts into the martian cryosphere will be an increase in abundance of these minerals.

In this way, impacts may have played a biologically important role on Mars by providing potential sites for the growth and long-term survival of life, including protection from the potentially detrimental environmental consequences of a progressively colder climate, high UV irradiation, atmospheric oxidants, and large surface-sterilizing impacts. Hypothetically, the survival of life would have been greatly aided by its ability to spread from

one habitable hydrous environment to another via the migratory pathways provided by the presence of sub-permafrost aquifers. The biological potential of these environments makes impact craters, especially those formed in the Noachian and Hesperian, good locations to search for physical and biogeochemical evidence of early Martian life.

Acknowledgment

This work was supported, in part, by NASA Mars Fundamental Research grants NNX07AK42G (D.A.K., S.P.S.) and NNX09AL25G (A.H.T., J.F.); by NASA MDAP grant number NNX09AI42G (P.J.M.); by NASA Planetary Geology and Geophysics grant NNH07DA001N (H.E.N.); by NASA Mars Science Laboratory project (R.C.W.) and Mars Fundamental Research Grant NNH10AO83I (D.V.); and a NASA Astrobiology Institute Director's Discretionary Fund award to O.A. We thank Bethany Ehlman, Bob Craddock and an anonymous reviewer for thoughtful reviews. This is Lunar and Planetary Institute (LPI) contribution #1668.

References

Abramov, O., 2006. Impact-Induced Hydrothermal Activity on Earth and Mars. Ph.D. Thesis, University of Arizona, Tucson, AZ.
Abramov, O., Kring, D.A., 2005. Impact-induced hydrothermal activity on Early Mars. J. Geophys. Res. 110 (E12S09)http://dx.doi.org/10.1029/2005JE002453.
Abramov, O., Mojzsis, S.J., 2009. Microbial habitability of the Hadean Earth during the late heavy bombardment. Nature 459, 419–422.
Ahrens, T.J., O'Keefe, J.D., 1987. Impact on the Earth, ocean and atmosphere. Int. J. Impact Eng. 5, 13–32.
Allen, C.C., 1979. Areal distribution of Martian rampart craters. Icarus 39, 111–123.
Arvidson, R.E., Squyres, S.W., Anderson, R.C., Bell III, J.F., Blaney, D., 58 co-authors, 2007. Overview of the Spirit Mars Exploration Rover Mission to Gusev Crater: landing site to Backstay Rock in the Columbia Hills. J. Geophys. Res. 111, E02S01, http://dx.doi.org/10.1029/2005JE02499.
Barlow, N.G., 1990. Constraints on early events in Martian History as derived from the cratering record. J. Geophys. Res. 95, 14191–14201.
Barlow, N.G., 2005. A review of Martian impact crater ejecta structures and their implications for target properties. In: Kenkmann, T., Hörz, F., Deutsch, A. (Eds.), Large Meteorite Impacts III, Geological Society of America Special Paper 384, pp. 433–442.
Barlow, N.G., 2006. Impact craters in the northern hemisphere of Mars: layered ejecta and central pit caracteristics. Meteoritics Planet. Sci. 41, 1425–1436.
Barnhart, C.J., Nimmo, F., Travis, B.J., 2010. Geochemical and geomorphological effects on post-impact hydrothermal systems incorporating freezing. Icarus 208, 101–117.
Bennett, J. and Shostak, S., 2007. Life in the Universe. San Francisco (Pearson), 485 pp.
Bibring, J.-P., Langevin, Y., Gendrin, A., Gondet, B., Poulet, F., Berthé, M., Soufflot, A., Arvidson, R., Mangold, N., Mustard, J.F., Drossart, P., the OMEGA team, 2005. Mars surface diversity as revealed by the OMEGA/Mars express observations. Science 307, 1576–1581.
Bibring, J.-P., Langevin, Y., Mustard, J.F., Poulet, F., Arvidson, R., Gendrin, A., Gondet, B., Mangold, N., Pinet, P., Forget, F., the OMEGA team, 2006. Global mineralogical and aqueous Mars history derived from OMEGA/Mars express data. Science 312, 400–404.
Bridges, J.C., Schwenzer, S.P., 2011. The nakhlite impact hydrothemal cell: mineralogy, fluid and habitability. In: Proceedings of the International Conference Exploring Mars Habitability, June 13–15, 2011, Lisbon, Portugal.
Bridges, J.C., Schwenzer, S.P., 2012. The nakhlite hydrothermal brine. In: Proceedings of the 43th Lunar and Planetary Science Conference, Abstract #2328, Houston.
Byrne, S., Dundas, C.M., Kennedy, M.R., Mellon, M.T., McEwwn, A.S., Cull, S.C., Daubar, I.J., Shean, D.E., Seelos, K.D., Murchie, S.L., Cantor, B.A., Arvidson, R.E., Edgett, K.S., Reufer, A., Thomas, N., Harrison, T.N., Posiolova, L.V., Seelos, F.P., 2009. Distribution of mid-latitude ground ice on Mars from new impact craters. Science 325, 1674–1676.
Carr, M.H., 1986. Mars: A Water-Rich Planet? Icarus 68, 187–216.
Carr, M.H., 1996. Water on Mars. University Press, New York–Oxford.
Carr, M.H., 1999. Retention of an atmosphere on early Mars. J. Geophys. Res. 104, 21897–21909.
Carr, M.H., 2006. The Surface of Mars. University Press, Cambridge.
Carter, J., Poulet, F., Bibring, J.-P., Murchie, S., 2010. Detection of hydrated silicates in crustal outcrops in the northern plains of Mars. Science 328, 1682–1686.
Changela, H.G., Bridges, J.C., 2010. Alteration assemblages in the nakhlites: variation with depth on Mars. Meteoritics Planet. Sci. 45, 1847–1867.
Clark, B.C., Van Hart, D.C., 1981. The salts of Mars. Icarus 45, 370–378.
Clifford, S.M., 1991. The role of thermal vapor diffusion in the subsurface hydrologic evolution of Mars. Geophys. Res. Lett. 18, 2055–2058.
Clifford, S.M., 1993. A model for the hydrologic and climate behaviour of water on Mars. J. Geophys. Res. 98, 10973–11016.
Clifford, S.M., Lasue, J., Heggy, E., Boisson, J., McGovern, P., Max, M., 2010. The depth of the Martian cryosphere: revised estimates and implications for the existence and detection of subpermafrost groundwater. J. Geophys. Res., 115, http://dx.doi.org/10.1029/2009JE003462.
Cockell, C.S., Balme, M., Bridges, J.C., Schwenzer, S.P., 2012. The search for uninhabitated habitats in Mars. Icarus 217, 184–193, http://dx.doi.org/10.1016/j.icarus.2011.10.025.
Cockell, C.S., Barlow, N.G., 2002. Impact excavation and the search for subsurface life on Mars. Icarus 155, 340–349.
Collins, G.S., Melosh, H.J., Morgan, J.V., Warner, M.R., 2002. Hydrocode simulations of chicxulub crater collapse and peak-ring formation. Icarus 157, 24–33.
Craddock, R.A., Howard, A.D., 2002. The case for rainfall on a warm, wet early Mars. J. Geophys. Res., 107, http://dx.doi.org/10.1029/2001JE001505.
Craddock, R.A., Maxwell, T., 1993. Geomorphic evolution of the martian highlands through ancient fluvial processes. J. Geophys. Res. 98, 3453–3468.
Deer, W.A., Howie, R.A. & Zusman, J., 1992. An Introduction to Rock-Forming Minerals. Essex (Longman). 696 pp.
Dekov, V.M., Kamenov, G.D., Stummeyer, J., Thiry, M., Savelli, C., Shanks, W.C., Fortin, D., Kuzmann, Ernö, Vértes, A., 2007. Hydrothermal nontronite formation at Eolo Seamount (Aeolian volcanic arc, Tyrrhenian Sea). Chem. Geol., 245.
Dreibus, G., Jochum, K.H., Palme, H., Spettel, B., Wlotzka, F., Wänke, H., 1992. LEW 88516: A meteorite compositionally close to the ''Martian mantle''. Meteoritics 27, 216–217.
Edwards, C.S., Christensen, P.R., Hamilton, V.E., 2008. Evidence for extensive olivine-rich basalt bedrock outcrops in Ganges and Eos chasmas, Mars. J. Geophys. Res., 113, http://dx.doi.org/10.1029/2008JE003091.
Ehlmann, B.L., Mustard, J.F., Bishop, J.L., Swayze, G.A., Roach, L.H., Clark, R.N., Milliken, R.E., Poulet, F., Murchie, S.L., the MRO CRISM Team, 2008a. Distinct provinces of aqueous alteration in the Western Isidis region identified with MRO-CRISM. Lunar Planet. Sci.. XXXIX, Abstract #2326; Houston.
Ehlmann, B.L., Mustard, J.F., Fassett, C.I., Schon, S.C., Head III, J.W., Marais, D.J., Grant, J.A., Murchie, S.L., 2008b. Clay minerals in delta deposits and organic preservation potential on Mars. Nat. Geosci. 1, 355–358.
Ehlmann, B.L., Mustard, J.F., Bishop, J.L., Swayze, G.A., Clark, R.N., Bishop, J.L., Poulet, F., Des Marais, D.J., Roach, L.H., Milliken, R.E., Wray, J.J., Barnouin-Jha, O., Murchie, S.L., 2009. Identification of hydrated silicate minerals on Mars using MRO-CRISM: geologic context near Nili Fossae and implications for aqueous alteration. J. Geophys. Res., 114, http://dx.doi.org/10.1029/2009JE003339.
Ehlmann, B., Mustard, J.F., Murchie, S.L., 2010. Geologic setting of serpentine deposits on Mars. Geophys. Res. Lett. 37 http://dx.doi.org/10.1029/2010GL042596.
Floran, R.J., Prinz, M., Hlava, P.F., Keil, K., Nehru, C.E., Hinthorne, J.R., 1978. The Chassigny meteorite: a cumulate dunite with hydrous amphibole-bearing melt inclusions. Geochim. Cosmochim. Acta 42, 1213–1229.
Filiberto, J., Schwenzer, S.P., 2011. Hydrothermal alteration mineralogy of Home Plate: thermochemical constraints for their formation conditions. In: Proceedings of the Planetary Science Conference, XLII: # 2072.
Gleason, J.D., Kring, D.A., Hill, D.H., Boynton, W.V., 1997. Petrography and bulk chemistry of Martian lherzolithe LEW88516. Geochim. Cosmochim. Acta 61, 4007–4014.
Grauby, O., Petit, S., Decarreau, A., Baronnet, A., 1994. The nontronite-saponite series: an experimental approach. Eur. J. Mineral. 6, 99–112.
Hahn, B.C., McLennan, S.M., Klein, E.C., 2011. Martian surface heat production and crustal heat flow from Mars Odyssey Gamma-Ray spectrometry. Geophys. Res. Lett., **38**, http://dx.doi.org/10.1029/2011GL047435.
Harder, H., 1976. Nontronite synthesis at low temperatures. Chemical Geology 18, 169–180.
Hecht, M.H., Kounaves, S.P., Quinn, R.C., West, S.J., Young, S.M.M., Ming, D.W., Catling, D.C., Clark, B.C., Boynton, W.V., Hoffman, J., DeFlores, L.P., Gospodinova, K., Kapit, J., Smith, P.H., 2009. Detection of perchlorate and the soluble chemistry of Martian soil at the phoenix landing site. Science 325, 64–67.
Hobbs, P.V., 1974. Ice Physics. Clarendon Press, Oxford, England.
Holsapple, K.A., Schmidt, R.M., 1982. On the scaling of crater dimensions 2. J. Geophys. Res. 87, 1849–1870.
Horner, J., Mousis, O., Petit, J.-M., Jones, B.W., 2009. Differences between the impact regimes of the terrestrial planets: implications for primordial D:H ratios. Planet. Space Sci. 57, 1338–1345.
Ivanov, B.A., Pierazzo, E., 2011. Impact cratering in H_2O-bearing targets on Mars: thermal field under craters as starting conditions for hydrothermal activity. Meteorit. Planet. Sci. 46, 601–619.
Kieffer, S.W., Simonds, C.H., 1980. The role of volatiles and lithology in the impact cratering process. Rev. Geophys. Space Phys. 18, 143–181.
Koeppen, W.C., Hamilton, V.E., 2008. Global distribution, composition, and abundance of olivine on the surface of Mars from thermal infrared data. J. Geophys. Res., 113, http://dx.doi.org/10.1029/2007JE002984.
Kring, D.A., Cohen, B.A., 2002. Cataclysmic bombardment throughout the inner solar system 3.9–4.0 Ga. J. Geophys. Res. 107 (E) http://dx.doi.org/10.1029/2001JE001529. 4-1–4-6.
Laskar, J., Correia, A.C.M., Gastineau, M., Joutel, F., Levrard, B., Robutel, P., 2004. Long term evolution and chaotic diffusion of the insolation quantities of Mars. Icarus 170, 343–364.

Manning, C.E., Ingebritsen, S.E., 1999. Permeability of the continental crust: implications of geothermal data and metamorphic systems. Rev. Geophys. 37, 127–150.
Marzo, G.A., Davila, A.F., Tornabene, L.L., Dohm, J.M., Fairén, A.G., Gross, C., Kneissl, T., Bishop, J.L., Roush, T.L., McKay, C.P., 2010. Evidence for Hesperian impact-induced hydrothermalism on Mars. Icarus 208, 667–683.
Masursky, H., Boyce, J.M., Dial, A.L., Schaber, G.G., Strobell, M.E., 1977. Classification and time of formation of the Martian channels based on Viking data. J. Geophys. Res. 82, 4016–4038.
McGovern, P.J., Solomon, S.C., Smith, D.E., Zuber, M.T., Simons, M., Wieczorek, M.A., Phillips, R.J., Neumann, G.A., Aharonson, O., Head, J.W., 2004. Correction to "Localized gravity/topography admittance and correlation spectra on Mars: implications for regional and global evolution. J. Geophys. Res., 109, http://dx.doi.org/10.1029/2004JE002286.
Melosh, H.J., 1989. Impact Cratering. Oxford University Press, New York.
Milliken, R.E., Bish, D.L., 2010. Sources and sinks of clay minerals on Mars. Philos. Mag. 90, 2293–2308.
Milliken, R.E., Grotzinger, J.P., Thomson, B.J., 2010. Paleoclimate of Mars as captured by the stratigraphic record in Gale Crater. Geophys. Res. Lett., 37, http://dx.doi.org/10,1029/2009GL041870.
Minissale, A., Vaselli, O., Chandrasekharam, D., Magro, G., Tassi, F., Casiglia, A., 2000. Origin and evolution of 'intracratonic' thermal fluids from central-western peninsular India. Earth Planet. Sci. 181, 377–394.
Morris, R.V., Golden, D.C., Ming, D.W., Graff, T.G., Arvidson, R.E., Wiseman, S.M., Lichtenberg, K.A., Cull, S., 2009. Visible and near-IR reflectance spectra for smectite, sulfate and perchlorate under dry conditions for interpretation of Martian surface mineralogy. In: Proceedings of the 40th Lunar and Planetary Science Conference, Abstract #2317, Houston.
Murchie, S.L., Mustard, J.F., Ehlmann, B.L., Milliken, R.E., Bishop, J.L., 12 co-authors, 2009a. A synthesis of Martian aqueous mineralogy after 1 Mars year of observations from the Mars Reconnaissance orbiter. J. Geophys. Res., 114, ht tp://dx.doi.org/10.1029/2009JE003342.
Murchie, S.L., Seelos, F.P., Hash, C.D., Humm, D.C., Malaret, E., 18 co-authors, 2009b. Compact reconnaissance imaging spectrometer for mars investigation and dataset from the Mars Reconnaissance Orbiter's primary science phase. J. Geophys. Res., 114, http://dx.doi.org/10.1029/2009JE003344.
Mustard, J.F., Murchie, S., Pelkey, S.M., Ehlmann, B.L., Milliken, R.E., 31 co-authors, 2008. Hydrated silicate minerals on Mars observed by the Mars Reconnaissance Orbiter CRISM instrument. Nature 454, 305–309.
Newsom, H.E., Hagerty, J.J., Thorsos, I.E., 2001. Location and sampling of aqueous and hydrothermal deposits in Martian impact craters. Astrobiology 1, 71–88.
Norman, M.D., Nemchin, A.A., 2012. Heavy Bombardment of the Moon at ~4.2 Ga: evidence from Ages of Lunar Melt Breccias and Zircons. In: Proceedings of the 43rd Lunar and Planetary Science Conference, Abstract #1368, Houston.
Onstott, T.C., McGown, D.J., Bakermans, C., Ruskeeniemi, T., Ahonen, L., Telling, J., Soffientino, B., Pfiffner, S.M., Sherwood-Lollar, B., Frape, S., Stotler, R., Johnson, E.J., Vishnivetskaya, T.A., Rothmel, R., Pratt, L.M., 2009. Microbial communities in subpermafrost saline fracture water at the Lupin Au Mine, Nunavut, Canada. Microbiol. Ecol. 58, 786–807.
Osinski, G.R., 2006. Effect of volatiles and target lithology on the generation and emplacement of impact crater fill and ejecta deposits on Mars. Meteorit. Planet. Sci 41, 1571–1586.
Osterloo, M.M., Hamilton, V.E., Bandfield, J.L., Glotch, T.D., Balridge, A.M., Christensen, P.R., Tornabene, L.L., Anderson, F.S., 2008. Chloride-bearing materials in the southern highlands of Mars. Science 319, 1651–1654.
Oze, C., Sharma, M., 2005. Have olivine, will gas: serpentinization and the abiogenetic production of methane on Mars. Geophys. Res. Lett. 32, http://dx.doi.org/10.1029/2005GL022691.
Pierazzo, E., Melosh, H.J., 2000. Melt production in oblique impacts. Icarus 145, 252–261.
Pierazzo, E., Artemieva, N.A., Ivanov., B.A., 2005. Starting conditions for hydrothermal systems underneath Martian craters: hydrocode modeling. In: Kenkmann, T., Hörz, F., Deutsch, A. (Eds.), Large Meteorite Impacts. Geological Society of America, pp. 443–457. Special Paper 384.
Pike, R.J., 1988. Geomorphology of Impact Craters on Mercury. In: Chapman, C.R., Matthews, F., Vilas, F. (Eds.), Mercury. University of Arizona Press, pp. 165–273.
Piranjo, F. 2009. Hydrothermal Processes and Mineral Systems, Springer, p. 133, 624.
Pollack, J.B., Kasting, J.F., Richardson, S.M., Poliakoff, K., 1987. The case for a wet, warm, climate on early Mars. Icarus 71, 203–224.
Poulet, F., Bibring, J.-P., Mustard, J.F., Gendrin, A., Mangold, N., Langevin, Y., Arvidson, R.E., Gondet, B., Gomez, C., 2005. and the OMEGA Team, 2005. Phyllosilicates on Mars and implications from early martian climate. Nature 438, 623–627.
Poulet, F., Gomez, C., Bibring, J.-P., Langevin, Y., Gondet, B., Pinet, P., Belluci, G., Mustard, J.F., 2007. Martian surface mineralogy from Observatoire pour la Minéralogie, l'Eau, les Glaces et l'Activité on board the Mars Express spacecraft (OMEGA/MEx): Global mineral maps. J. Geophys. Res., 112, http://dx.doi.org/10.1029/2006JE002840.
Reed, M.H., Spycher, N.F., 2006. Users Guide for CHILLER: A Program for Computing Water-Rock Reactions, Boiling, Mixing and Other Reaction Processes in Aqueous-Mineral-Gas systems and Minplot Guide, third ed. University of Oregon, Oregon 67 pp.
Reiss, D., Gasselt, S., van, Hauber, E., Michael, G., Jaumann, R., Neukum, G., 2006. Ages of rampart craters in equatorial regions on Mars: implications for the past and present distribution of ground ice. Meteorit. Planet. Sci. 41, 1437–1452.
Schwenzer, S.P. 2011. Quantifying low temperature production of methane on Mars. In: Proceedings of the Planetary Science Conference, XLII: #1803.
Schwenzer, S.P., Bridges, J.C., 2011. The secondary mineral forming fluid in the nakhlites. In: Proceedings of the Meteoritical Society Meeting, London, #5276.
Schwenzer, S.P., Kring., D.A., 2009a. Impact-generated hydrothermal systems: capable of forming phyllosilicates on Noachian Mars. Geology 37, 1091–1094.
Schwenzer, S.P., Kring, D.A., 2009b. Impact-generated hydrothermal alteration on Early Mars in presence of CO_2. Meteorit. Planet. Sci. 44, A188. (abstract #5262).
Schmidt, R.M., Housen, K.R., 1987. Some recent advances in the scaling of impact and explosion cratering. Int. J. Impact Eng. 5, 543–560.
Squyres, S.W., 2011. Vision and Voyages for Planetary Science in the Decade 2013–2022. Committee on the Planetary Science Decadal Survey, National Research Council. 〈http://www.nap.edu/catalog/13117.html〉.
Strom, R.G., Malhotra, R., Ito, T., Yoshida, F., Kring, D.A., 2005. The origin of planetary impactors in the inner solar system. Science 309, 1847–1849.
Stucki, J.W., 2006. Properties and behaviour of iron in clay minerals. In: Bergaya, F., Theng, B.K.G., Lagaly, G. (Eds.), Handbook of Clay Science—Developments in Clay Science, vol. 1; 2006, pp. 423–475.
Tosca, N.J., Knoll, A.H., McLennan, S.M., 2008. Water activity and the challenge for life on early Mars. Science 320, 1204–1207.
Varnes, E.S., Jakosky, B.M., McCollom, T.M., 2003. Biological potential of martian hydrothermal Systems. Astrobiology 3, 407–414.
Ward, W.R., 1979. Present obliquity oscillations of Mars—fourth-order accuracy in orbital E and I. J. Geophys. Res. 84, 237–241.
Warren, P.H., Kallemeyn, G.W., 1996. Siderophile trace elements in ALH84001, other SNC meteorites and Eucrites: evidence of heterogeneity, possibly time-linked, in the mantle of Mars. Meteorit. Planet. Sci. 31, 97–1005.
Zolotov, M.Yu., Shock, E.L., 1999. Abiotic synthesis of polycyclic aromatic hydrocarbons on Mars. J. Geophys. Res. 104, 14033–14049.